Sediment transport associated with morphological beach changes forced by irregular asymmetric, skewed waves

F. Grasso,[1,2] H. Michallet,[1] and E. Barthélemy[1]

Received 26 July 2010; revised 8 November 2010; accepted 3 January 2011; published 23 March 2011.

[1] The waveshape effects on sediment transport are investigated for cross-shore beach profile changes. This study is based on experiments performed in the Laboratoire des Ecoulements Géophysiques et Industriels wave flume for irregular waves. The interest of such experiments resides in presenting complex combinations of wave skewness and asymmetry in bed load, ripple, and sheet flow regimes. Net sediment transport rates on typical beach morphodynamics are analyzed in regard to wave skewness and asymmetry, undertow, and ripple occurrence. Onshore bar migration is mainly associated with onshore-directed sediment transport, whereas terrace profile and offshore bar formation correspond to offshore sediment transport. As for natural beaches, energetic (moderate) wave climates mostly induce offshore (onshore) sediment fluxes. For a given significant wave height, an increase (decrease) in the wave climate peak period is associated with an increase (decrease) in wave skewness and leads mostly to offshore (onshore) sediment fluxes. The experiments are fully characterized by unsteady behavior. Consequently, several conditions exhibit phase-lag effects where the sediment is mobilized by the wave crest and transported by the following trough, which produces a net offshore transport even for a weak undertow. The presence of ripples clearly contributes to enhance this behavior. An original concept, due to its application to skewed asymmetric irregular waves, presents the important interaction between wave nonlinearities driving the sediment fluxes. The net sediment transport rate under strongly skewed waves is either offshore directed due to phase-lag effects or onshore directed when the wave asymmetry is large enough. Both these mechanisms probably largely contribute to bar formation and migration.

Citation: Grasso, F., H. Michallet, and E. Barthélemy (2011), Sediment transport associated with morphological beach changes forced by irregular asymmetric, skewed waves, *J. Geophys. Res.*, *116*, C03020, doi:10.1029/2010JC006550.

1. Introduction

[2] The prediction of sediment transport due to wave action is of major concern to the coastal scientific and engineering community. Tools for predicting sediment fluxes range from simple parameterized formulas to CPU time-consuming physical process modeling (see, e.g., the comparison of sediment transport models by *Davies et al.* [2002]). Simple morphodynamic models, based on empirical approaches or data-driven neural network models, are investigated to predict long-term sandbar migration [e.g., *Pape et al.*, 2010b, 2010a]. However, most of the simplest models are generally based on an "energetic" approach [*Bagnold*, 1966; *Bowen et al.*, 1980; *Bailard*, 1981] for which the energy expended by steady flows for transporting sediment is proportional to the total dissipation. Although such models successfully predict offshore bar migration, they fail to predict onshore migration [*Gallagher et al.*, 1998].

[3] *Elgar et al.* [2001] highlighted the importance of wave asymmetry for onshore bar migration, leading to several authors incorporating this process in their sediment transport models [*Drake and Calantoni*, 2001; *Hoefel and Elgar*, 2003; *Hsu et al.*, 2006; *Ruessink et al.*, 2007; *Castelle et al.*, 2010]. Waveshapes inducing velocity skewness (for sharp, high crests and broad, shallow troughs) and velocity asymmetry (for forward pitched of saw tooth-type waves) are usually responsible for sediment transport in the direction of wave propagation (onshore). Typical skewed waves in the shoaling zone induce high crest velocities in onshore direction that mobilize and transport more sediment than the offshore-directed trough velocities [*Hsu and Hanes*, 2004; *Marino-Tapia et al.*, 2007]. Additionally, the strong fluid acceleration induced by the steep front faces of asymmetric waves enhances sediment mobilization by the crests, further favoring the onshore sediment flux [*Drake and Calantoni*, 2001; *Terrile et al.*, 2006]. Such physics is drawn upon to explain the bar formation mechanism [e.g., *Roelvink and Stive*, 1989] where sandbars are the result of sediment

[1]Laboratoire des Ecoulements Géophysiques et Industriels, UJF/G-INP/CNRS, Grenoble, France.
[2]Institute for Marine and Atmospheric Research, Department of Physical Geography, Faculty of Geosciences, Utrecht University, Utrecht, Netherlands.

0148-0227/11/2010JC006550

transport convergence produced by onshore-directed fluxes due to wave asymmetries, and offshore-directed fluxes due to the wave-induced mean current, i.e., undertow.

[4] The undertow is usually considered to be the main mechanism distributing sediment offshore, in correlation with wave stirring [*Marino-Tapia et al.*, 2007] that can be enhanced by breaking wave turbulence [*Roelvink and Stive*, 1989; *van Thiel de Vries et al.*, 2008]. The net sediment transport associated with purely skewed waves, however, may also be offshore directed, due to phase lag between the mobilization and the transport of sediment [*Dohmen-Janssen et al.*, 2002]. In this case, the sediment mobilized by the crest is transported by the following trough before it settles. This mechanism is characterized by the phase-lag parameter [*Dohmen-Janssen et al.*, 2002]:

$$P_s = \frac{\delta_s \omega}{w_s} = 2\pi \frac{\Delta t_{settl}}{T} \quad (1)$$

where $\omega = 2\pi/T$ with T the wave period, w_s the sediment settling velocity, Δt_{settl} the time needed for particles for settling to the bed, and δ_s the sheet flow layer, defined as

$$\delta_s = 13\ d_{50}\ \theta \quad (2)$$

for $d_{50} \geq 0.21$ mm, θ being the Shields number (dimensionless bed shear stress parameter). Following *Ribberink et al.* [2008], $P_s \geq 0.1$–0.3 indicates an unsteady behavior, for which phase-lag effects take place. The criterion $P_s \leq 0.1$–0.3 indicates that the settling time has to be an order of magnitude smaller than the wave period for a quasi-steady behavior to dominate.

[5] According to *Nielsen* [1992], phase-lag effects can occur for both vortex ripple and sheet flow regimes. These sediment transport regimes may be characterized by the Shields number θ, representing the ratio of the bed shear stress to the submerged weight of sediment. It is well known that sediment starts to be mobilized close to $\theta \approx 0.05$ for rough turbulent boundary layers. For $0.05 \leq \theta \leq 1$ the sediment is first transported by bed load and may be followed by the development of vortex ripples. Beyond $\theta \approx 1$, the ripples are washed out and the sediment moves as a granular sheet with a thickness ranging from a few grain diameters up to several tenth of grain diameters, defined the sheet flow regime. The presence of ripples may also be characterized by the mobility number ψ. *O'Donoghue et al.* [2006] conducted large-scale experiments in two oscillatory flow tunnels to study ripple regimes. They concluded that for irregular flows, the ripple regime occurs below $\psi \approx 190$ and flat bed occurs above $\psi \approx 300$. *Ribberink et al.* [2008] defined this limit around $\psi \approx 100$–200. Vortex ripples induce strong perturbations of the bottom boundary layer and thus deeply affect the sediment transport. For instance *van der Werf et al.* [2007] analyzed the sediment flux over full-scale ripples in regular oscillatory flows. They found that asymmetric vortex formation, induced by the asymmetric free stream velocity, produces steady circulation cells with dominant offshore mean flow up the ripple lee slope. Hence, ripple occurrence enhances the sediment suspension and contributes to offshore sediment transport [e.g., *Nielsen*, 1992].

[6] Recent experiments have been performed using oscillatory flow tunnels in order to analyze the effect of skewed asymmetric waves on sediment transport [*Silva et al.*, 2011; *van der A et al.*, 2010]. Based on this type of experiment and using a 1DV-RANS "advection/diffusion" model, *Ruessink et al.* [2009] explored the influence of different combinations of velocity skewness and asymmetry on the net sediment flux. They show that phase-lag effects reduce the wave-induced transport rates under oscillatory flow dominated by velocity skewness; the net rates are then dominated by the transport rates induced by the turbulence asymmetry generated streaming, and are against the direction of wave advance. With an increase in velocity asymmetry, phase-lag effects start to increasingly enhance the transport rates in the direction of wave advance: sand entrained into the flow under the negative wave half-cycle has not settled prior to flow reversal and is transported during the positive wave half-cycle. These mechanisms were confirmed from the analysis of sediment fluxes measurements presented by *Ruessink et al.* [2011], while *van der A et al.* [2010] showed even larger phase-lag effects for a finer sand.

[7] Whereas most of the above mentioned studies involved oscillatory flows under regular waves, fewer studies have focused on the influence of asymmetries of irregular waves on sediment transport. Moreover, the effects of wave asymmetries on sediment transport over sloping beds had received little attention. Analyzing the interplay of skewness and asymmetry in field measurements is a difficult task. The controlled conditions of physical modeling, however, provide an interesting alternative [*Scott et al.*, 2009; *Yu et al.*, 2010]. The analysis presented herein is based on measurements carried out in the Laboratoire des Ecoulements Géophysiques et Industriels (LEGI) flume [*Grasso et al.*, 2009a]. This small-scale flume enables the generation of irregular skewed asymmetric waves above a changing cross-shore beach profile. *Grasso et al.* [2009a, 2009b, 2011] showed that such small-scale laboratory experiments using lightweight sediment can reproduce natural beach morphodynamics. *Aagaard et al.* [2002] described the sediment transport by a parameterized formulation using the Shields number, relative water depth, wave orbital velocity, relative wave height, and bed slope. These parameters are used to link the undertow, incident wave skewness and cross correlation between orbital velocity and sediment concentration. Using wave measurements all along various beach profiles, the purpose of the present study is to characterize the net sediment transport rate with regard to the wave height, wave skewness and asymmetry, Shields number, undertow, and bottom profile. The main contribution of this paper is to present a concept, describing sediment transport associated with morphological beach changes, forced by irregular skewed and asymmetric waves.

[8] The methods are detailed in section 2, describing the experimental setup and the characterization of the bed form. Results are presented in section 3, investigating typical beach profile changes under particular wave conditions. The discussion and conclusions will be addressed in section 4.

2. Experimental Setup and Methods

2.1. Experimental Setup

[9] The experimental setup is described in detail by *Grasso* [2009]. The main characteristics are recalled here. The experiments were carried out in the 36 m long and

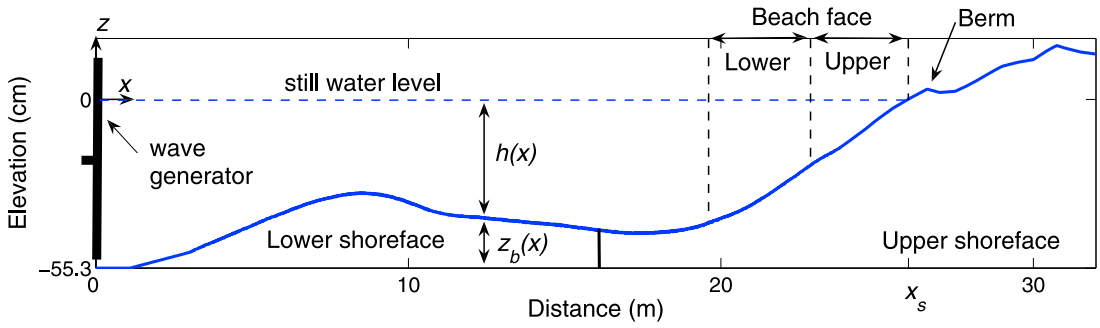

Figure 1. Schematic diagram of the LEGI wave flume: $h(x)$ and $z_b(x)$ are the mean water depth and the bottom elevation at the cross-shore position x. Vertical dashed lines delineate lower and upper beach faces. The vertical solid line (at x = 16.5 m) delineates lower (left-hand side) and upper (right-hand side) shoreface parts, and x_s is the shoreline position.

55 cm wide LEGI flume, equipped with a piston wave generator (see Figure 1). The still water depth at the wave maker is 55.3 cm. The sloping bottom consists of loose material of low density (1.19 g cm^{-3}) with a median diameter d_{50} = 0.64 mm (corresponding settling velocity w_s = 2.1 cm s^{-1}). The Froude number, the Shields number and the Rouse number are of the same magnitude as those of natural environments [*Grasso et al.*, 2009a]. Time and length scale ratios are roughly 1/3 and 1/10, respectively. Irregular waves are generated using a JONSWAP spectrum (peak enhancement factor = 3.3). The water free surface elevations are measured with twelve capacitive wave probes. It is checked that the waves conform to the expected spectrum and that they follow a Rayleigh distribution 2 m downstream of the wave maker. Bottom profiles are recorded between wave runs using an acoustic profiler mounted on a motorized trolley. The generated wave climates (termed B-F) are characterized by their significant wave height H_s, peak period T_p, and the corresponding Dean number, defined as $\Omega = H_s/(T_p\ w_s)$ (Table 1).

2.2. Analysis Tools

[10] The bottom profile is the result of a trade off between mechanisms transporting sediment offshore and others contributing to onshore fluxes. The analysis is based on the change in hydrodynamic parameters across the beach profiles. A full hydrodynamic description of wave propagation and transformation on a cross-shore profile is intensively investigated by *Michallet et al.* [2011]. This study, using data from the LEGI flume experiments, discusses similarities between sea surface elevation and bottom velocity nonlinearities. It also provides a thorough comparison with results from a Boussinesq-type model [*Cienfuegos et al.*, 2010]. For long waves, the orbital wave velocity is at first order proportional to the free surface elevation, hence the crest-to-trough asymmetry or velocity skewness may be estimated as [e.g., *Doering and Bowen*, 1995]

$$Sk = \frac{\left\langle (\eta - \overline{\eta})^3 \right\rangle}{\left\langle (\eta - \overline{\eta})^2 \right\rangle^{3/2}} \tag{3}$$

where η is the free surface elevation, $\overline{\eta}$ the mean water level, and $\langle . \rangle$ the time averaging operator. This term is equivalent to Term 02 of *Marino-Tapia et al.* [2007]. The Stokes wave theory gives an insight into which flow parameters determine the skewness behavior in the shoaling zone. For shallow water conditions, the second-order Stokes wave free surface displacement writes

$$\frac{\eta}{H} = \frac{1}{2}\cos\omega t + \frac{3}{16}\frac{H}{h}\frac{1}{k^2h^2}\cos 2\omega t \tag{4}$$

where h is the water depth, H the wave height, k the wave number and ω the pulsation related to wave period T as $\omega = 2\pi/T$. This gives the following expression for the third-order moment $\overline{\eta^3}$ in shallow water conditions:

$$\frac{\overline{\eta^3}}{H^3} = \frac{9}{1024\,\pi^2}\frac{H}{h^2}gT^2 \tag{5}$$

where g is the gravitational acceleration.

[11] Note that expression (5) is proportional to the Ursell number. In turn, the wave skewness reads

$$Sk = 8^{3/2}\frac{\overline{\eta^3}}{H^3} \propto \frac{H}{h^2}T^2 \tag{6}$$

Consequently in the shoaling zone where H increases and h decreases, the skewness increases. Moreover, for given H

Table 1. Wave Conditions Used in This Study[a]

Experiment	Wave Climate	H_s (cm)	T_p (s)	Ω	Δt (h)	Observations
1	F	16	2	3.7	0.5	Onshore bar migration
2	C	16	3	2.5	1	Offshore bar formation
3	C	16	3	2.5	9.1	Terrace formation
4	C	16	3	2.5	11.5	Equilibrium profile
5	B	10.7	2	2.5	1.2	Barred profile
6–9	B	10.7	2	2.5	≈1	Barred profiles
10	C	16	3	2.5	0.7	Barred profile
11–14	C	16	3	2.5	≈2.5	Barred profiles
15	D	10.7	1.4	3.6	1.2	Shore accretion
16	B	10.7	2	2.5	1.9	Shore erosion
17	F	16	2	3.7	1.3	Shore accretion
18	C	16	3	2.5	1.3	Shore erosion
19	B	10.7	2	2.5	2	Equilibrium profile
20	E	12.5	1.6	3.7	1.5	Equilibrium profile

[a]Here Δt is the wave duration used to compute the net sediment transport rate.

and h, longer wave periods increase the wave skewness. The front-to-lee asymmetry can be characterized by the skewness of the acceleration [*Hsu et al.*, 2006]. Here we use an equivalent formulation, the third-order moment of the Hilbert transform [*Kennedy et al.*, 2000]:

$$As = \frac{\left\langle \mathcal{H}^3(\eta - \overline{\eta}) \right\rangle}{\left\langle (\eta - \overline{\eta})^2 \right\rangle^{3/2}} \tag{7}$$

where $\mathcal{H}$ is the Hilbert transform. The correlation between the nonlinearities deduced from surface elevations and near-bed velocity measurements has been evaluated for irregular waves breaking on a bar-trough topography [*Michallet et al.*, 2011]. The values of the velocity skewness and asymmetry are over predicted when deduced from the free surface elevations. However, the overall trend of wave skewness and wave asymmetry evolutions along the water depth variations is similar for both types of measurements.

[12] The undertow, partly compensating the wave breaking and crest forward fluid motion (i.e., Stokes drift), is estimated from the time-averaged continuity equation [*Dally and Brown*, 1995; *Michallet et al.*, 2011]:

$$\frac{\mathrm{d}}{\mathrm{d}x}[U(h + \overline{\eta})] + \frac{\mathrm{d}Q_W}{\mathrm{d}x} + \frac{\mathrm{d}Q_R}{\mathrm{d}x} = 0 \tag{8}$$

where U is the depth-averaged mean current (or undertow), Q_W is the volume flux per unit crest width associated with the organized wave motion, and Q_R is the fluid volume flux due to the roller. In the following we use the new roller model presented by *Michallet et al.* [2011], that computes Q_W and Q_R for estimating the undertow. In contrast to the roller model used by *Grasso et al.* [2009a], we do not use a wave driver here. The measured root mean square wave heights and the free surface elevations are directly used to force the undertow model. This avoids including uncertainties due to a wave driver in the calibration of the undertow model. *Michallet et al.* [2011] carried out velocity measurement in the near-bed region and showed that the roller model predicts accurate estimates of the undertow.

[13] In the present context, the Shields number measures whether the sediment is set in motion by the waves and what the transport regime is (bed load, sheet flow, suspension, etc). The fluid particle excursion at the bottom is

$$A = \frac{H_{rms}}{2 \sinh kh} \tag{9}$$

H_{rms} being the root mean square wave height and k the wave number. The Shields number is written as

$$\theta = \frac{1}{2} f_w \frac{(A\omega_m)^2}{g(\rho_s/\rho - 1)d_{50}} \tag{10}$$

where ρ and ρ_s are the water and sediment densities, and $\omega_m = 2\pi/T_m$ with T_m the mean wave period at the cross-shore position x. f_w is a wave friction factor which, according to *Swart* [1974], can be approximated as

$$f_w = \exp\left[5.213\left(\frac{2.5 \times d_{50}}{A}\right)^{0.194} - 5.977\right] \tag{11}$$

[14] To analyze the relative importance of the undertow on sediment transport, the Shields number is also computed using the crest and trough velocities. First, the near-bed orbital velocity is estimated from the free surface elevation in the framework of the shallow water theory:

$$u_{orb} = \frac{c}{h}(\eta - \overline{\eta}) - \frac{c}{h^2}\left((\eta - \overline{\eta})^2 - \overline{(\eta - \overline{\eta})^2}\right) \tag{12}$$

where $c = \sqrt{gh}$. According to *Michallet et al.* [2011], the second-order correction provides a better prediction of near-bed orbital velocities, especially in the wave crests. To account for the effect of the undertow, the mean component U in (8) is added to get an estimation of the near-bed velocity as $u_{tot} = u_{orb} + U$. The crest and trough Shields numbers are written as

$$\theta_{c,t} = \frac{1}{2} f_{w(c,t)} \frac{u_{c,t}^2}{g(\rho_s/\rho - 1)d_{50}} \tag{13}$$

where $u_{c,t}$ are the root mean square of the crest and trough velocities ($\max[u_{tot}]$ and $\min[u_{tot}]$), and $f_{w(c,t)}$ the friction factor computed with the crest and trough mean periods. If phase-lag effects do not occur, for $\theta_c/\theta_t > 1$ ($\theta_c/\theta_t < 1$) the sediment is more mobilized during the wave crests (troughs) and the net sediment transport is onshore (offshore) directed [*Dibajnia and Watanabe*, 1992].

[15] The mobility parameter is often used to define ripple occurrence and reads [e.g., *O'Donoghue et al.*, 2006]

$$\psi = \frac{u^2}{g(\rho_s/\rho - 1)d_{50}} \tag{14}$$

where $u = \sqrt{2}(A\omega_m)$ is the significant orbital velocity.

[16] Large horizontal pressure gradients associated with strongly asymmetric waves can lead to a fluidization of part of the bed layer and its mobilization during the positive wave half-cycle, a process known as "plug flow" [*Madsen*, 1974; *Foster et al.*, 2006]. *Sleath* [1999] performed experiments with an artificial sediment (of density $\rho_s/\rho = 1.141$ and median diameter $d_{50} = 0.7$ mm) similar to the one used in this study and characterized the potential occurrence of plug flow from the balance between the destabilizing force applied by the peak horizontal pressure gradient to the stabilizing force applied by gravity. The nondimensional Sleath parameter is defined as

$$S = \frac{(A\omega_m)\omega_m}{(\rho_s/\rho - 1)g} \tag{15}$$

Unlike the Shields number, the Sleath parameter does not depend on the grain size. In our case, most of the values

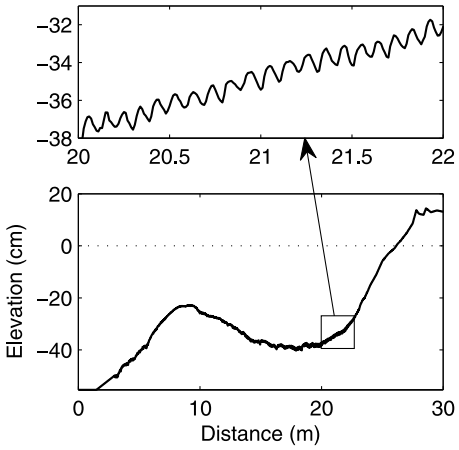

Figure 2. Barred beach profile presenting a typical rippled bed in the bar trough region.

range between 0.2 and 0.7, which fall in a domain where plug flow can occur. The domain where the plug flow should occur ($S > 0.76$ according to *Sleath* [1999]) corresponds to high Shields numbers ($\theta \geq 2$).

[17] The net sediment transport rate $\overline{q_s}$ is indirectly estimated from beach profile evolutions. Based on the difference between measured beach profiles and assuming a zero net transport rate at the wave maker ($x = 0$ m), the net sediment transport rate can be estimated using the sediment mass conservation equation:

$$\frac{\partial q_s}{\partial x} = -(1-p)\frac{\partial z_b}{\partial t} \tag{16}$$

where q_s is the instantaneous sediment transport rate, z_b is the bottom profile elevation at the cross-shore position x (see Figure 1), and $p = 0.4$ is the sediment bed porosity assumed to be homogeneous along the beach profile. During a given wave climate of duration Δt, the mean net sediment transport rate at a given cross-shore location is estimated by

$$\overline{q_s}(x) = \frac{1}{\Delta t}\int_t^{t+\Delta t} q_s(x,t)dt \tag{17}$$

$\overline{q_s} > 0$ ($\overline{q_s} < 0$) corresponds to net onshore (offshore) sediment transport.

2.3. Bed Form Characteristics

[18] Bed forms, and in particular ripples, play a crucial role in the sand suspension and net sediment transport processes [e.g., *Nielsen*, 1992; *O'Donoghue et al.*, 2006]. In this section, we present the methodology used to detect and determine bed ripple characteristics. Using the relation between ripple occurrence and the Shields number, we determined and classified the ripple regime in our small-scale experiments.

[19] The beach profiles measured by the acoustic profiler are used to analyze ripple characteristics. Figure 2 presents an example of ripples observed in the flume for a barred beach profile. Ripples are small-scale sedimentary features that we characterize by ξ which results from a high-pass filtering (running filter of 20 cm bandwidth) of the bottom elevation. The quantity ξ measures bed level fluctuations. A "zero down-crossing" method is then applied to this signal to extract ripple heights (H_r) and lengths (λ_r). These ripple characteristics are validated as long as the considered ripple is embedded in at least five adjacent ripples with less than 25% error in H_r and λ_r. This methodology was applied to the 20 beach profiles of experiments 1–20 presented in Table 1. In total, H_r, λ_r, and the associated Shields number θ (equation (10)) were obtained for 640 fully developed ripples.

[20] Ripple dimensions are presented in Figure 3, the ripple heights did not exceed 1.3 cm and the lengths ranged from 3 to 16 cm. Applying the 1/10 length scale factor to our experiments [*Grasso et al.*, 2009a], the measured ripple characteristics are in the range of those of the large ripples previously observed during large-scale physical experiments [e.g., *Ribberink and Al-Salem*, 1994] (Large Oscillating Water Tunnel, Delft, Netherlands) and in the field [e.g., *Hanes et al.*, 2001] (Duck beach, North Carolina). A data summary for experiments on ripple characteristics is presented by *Camenen* [2009]. Here, it is interesting to highlight that ripple dimensions (couple H_r, λ_r) are well contained in a restricted area, limited by

$$0.025\lambda_r \leq H_r \leq 0.15\lambda_r \tag{18}$$

Correspondingly, the ripple steepness H_r/λ_r ranges from 0.025 to 0.15 (Figure 3), in good agreement with previous studies. For instance *Bagnold* [1963] obtained a ripple steepness from 0 to 0.15, for *Camenen* [2009] the steepness ranged from 0.1 to 0.27, and *Masselink et al.* [2007] found values ranging from 0.05 to 0.17 for field measurements on Sennen Beach (Cornwall, England).

[21] When relating ripple dimensions to the Shields number, 90% of the ripples are observed for $0.27 \leq \theta \leq 0.94$, and 99% for $0.23 \leq \theta \leq 1.22$. This is in line with *Nielsen*'s [1992] conclusions, where $\theta \approx 1$ delineates ripple and sheet flow regimes for regular waves. Here, we assume that ripples can only occur for $\theta \leq 1.22$.

[22] Another way to check whether the ripples during these small-scale experiments were similar to those observed in nature consists of comparing the dimensionless ripple characteristics. Figure 4 clearly reveals that dimensionless ripple characteristics decrease with increasing mobility parameter. Ripples are hardly observed for $\psi \geq 200$, which corresponds to the washed-out ripple limits observed by *O'Donoghue et al.* [2006] of $\psi \geq 190$–300 and *Ribberink et al.* [2008] of $\psi \geq 100$–200.

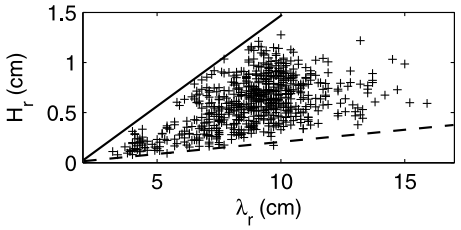

Figure 3. Ripple heights and lengths measured on the beach profiles of experiments 1–20 (640 ripples). The dashed line corresponds to $H_r/\lambda_r = 0.025$ and the solid line to $H_r/\lambda_r = 0.15$.

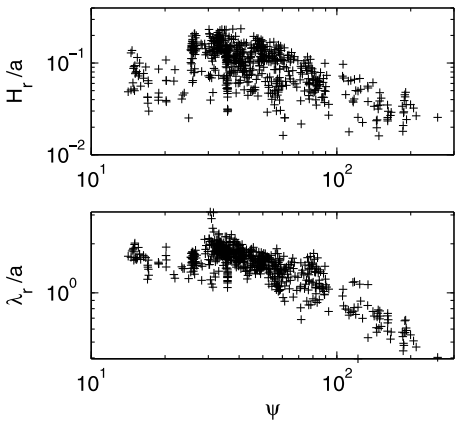

Figure 4. Dimensionless ripple characteristics versus the mobility parameter: $a = \sqrt{2}A$ is the significant particle excursion.

[23] Summarizing, ripple occurrence criteria based on the Shields and mobility numbers can be applied to the present experiments, and the threshold of $\theta = 1.22$ will be used for defining the limit between ripple and sheet flow regimes.

2.4. Phase-Lag Effects

[24] The experiments presented in this paper are characterized by Shields numbers θ ranging from 0.2 to 2.9, covering all the different sediment transport regimes. Phase-lag effects can occur for both ripple and sheet flow regimes and the phase-lag parameter was computed using the *Dohmen-Janssen et al.* [2002] formulation (1). This parameter is presented in Figure 5 for the 533 measurement points gathering experiments 1–20. $P_s \geq 0.3$ for most of the experiments, corresponding to unsteady behavior, during which phase-lag effects can occur. Hence, the latter are important processes to consider in this study.

3. Results

[25] The results are discussed by analyzing cross-shore variations of wave skewness *Sk* (3) and asymmetry *As* (7), Shields number θ, $\theta_{c,t}$ (10, 13), undertow *U* (8), net sediment transport rate $\overline{q_s}$ (17), root mean square wave height H_{rms}, and bed level fluctuation ξ. Experimental measurement points are depicted as symbols, and interpolated values are represented by lines.

3.1. Bar Formation and Migration

[26] Figures 6a–6i compare the cross-shore changes of the sediment transport parameters in the case of a sandbar migrating onshore at approximately 1.4 m h^{-1} (experiment 1 in Table 1). Figure 6i results from 30 min of the wave climate F. The bar maintains a typical forward pitched shape during migration. The net sediment transport is mostly onshore directed and reaches its maximum over the bar crest (Figure 6g). Thus, the bar migration is essentially driven by an onshore flux on the seaward side, and slight offshore flux in the bar trough. Waves are breaking on the bar (Figure 6a), which induces an undertow reaching its maximum slightly before the bar crest (Figure 6f). The undertow is mainly forced by the wave energy dissipated during breaking; *Grasso et al.* [2009a] highlighted very similar signatures between the undertow and the wave energy dissipation along the cross-shore beach profiles. The surf zone corresponds to a zone of large dissipation and is here readable through the undertow tendencies. In Figures 6a–6i, the surf zone is extending between the beginning of the wave height decay at $x \approx 15$ m and $x \approx 22$ m. Wave shoaling produces a clear increase in wave skewness, as predicted by (6), which reaches a maximum where wave dissipation is maximum (Figure 6b). Note that the wave breaking is associated with an increase in wave asymmetry (Figure 6c). The increasing water depth in the bar trough produces a rapid decay of the wave skewness and asymmetry, and undertow.

[27] Wave climate C was imposed during 1 h on a barred beach profile (Figures 6j–6r, experiment 2). Small sandbars of 1 m length scale on the lee side of the bar migrate offshore at approximately −0.4 m h^{-1} and nourish the main outer bar at $x \approx 8$ m. The associated sediment transport is mainly offshore directed, except at the bottom and the top of the beach. The outer bar clearly forms as the result of the sediment transport convergence, which is onshore directed from the seaward side of the bar, and offshore directed from the bar trough. The first breaking zone on the outer bar ($x \approx 8$ m) induces a moderate undertow compared to the second breaking zone on the upper beach face ($x \approx 22$ m). *Sk* and *As* exhibit a similar behavior as in the onshore bar migration case (Figures 6a–6i), but here with two breaking zones. Large values of *As* are observed close to the break points. Broken waves effectively have a "saw tooth" shape. Positive values of *As* in the bar trough indicate a trend for the waves to be pitched backward. Compared to *As*, *Sk* increases in the shoaling zone and remains large for a longer distance in the bar trough, but does not increase significantly during the second wave breaking. Kinematics of propagating and breaking waves on a barred beach is described in more detail by *Michallet et al.* [2011]. Here, similar tendencies for *As*, *U*, and θ are observed. These three parameters are linked to the breaking waves. *As* through the broken waveshape, *U* through the wave height decay (wave energy dissipation), and θ through the resulting sediment mobilization.

[28] For the two experiments presented here, the Shields number ranges from 0.4 to 2.3, corresponding to ripple and sheet flow transport regimes. It is readable in the plots of Figures 6h and 6q, where the bed level fluctuations ξ are larger in the bar trough, and smaller on the bar crest and on

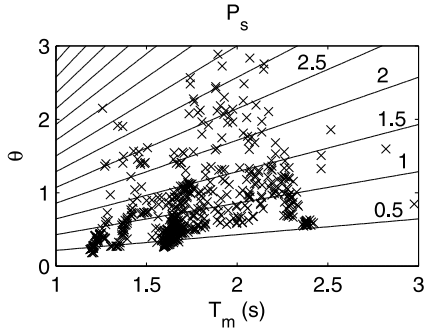

Figure 5. Phase-lag parameter P_s (isoline) versus Shields number θ and mean wave period T_p for all the experiments presented in this study (experiments 1–20, 533 points).

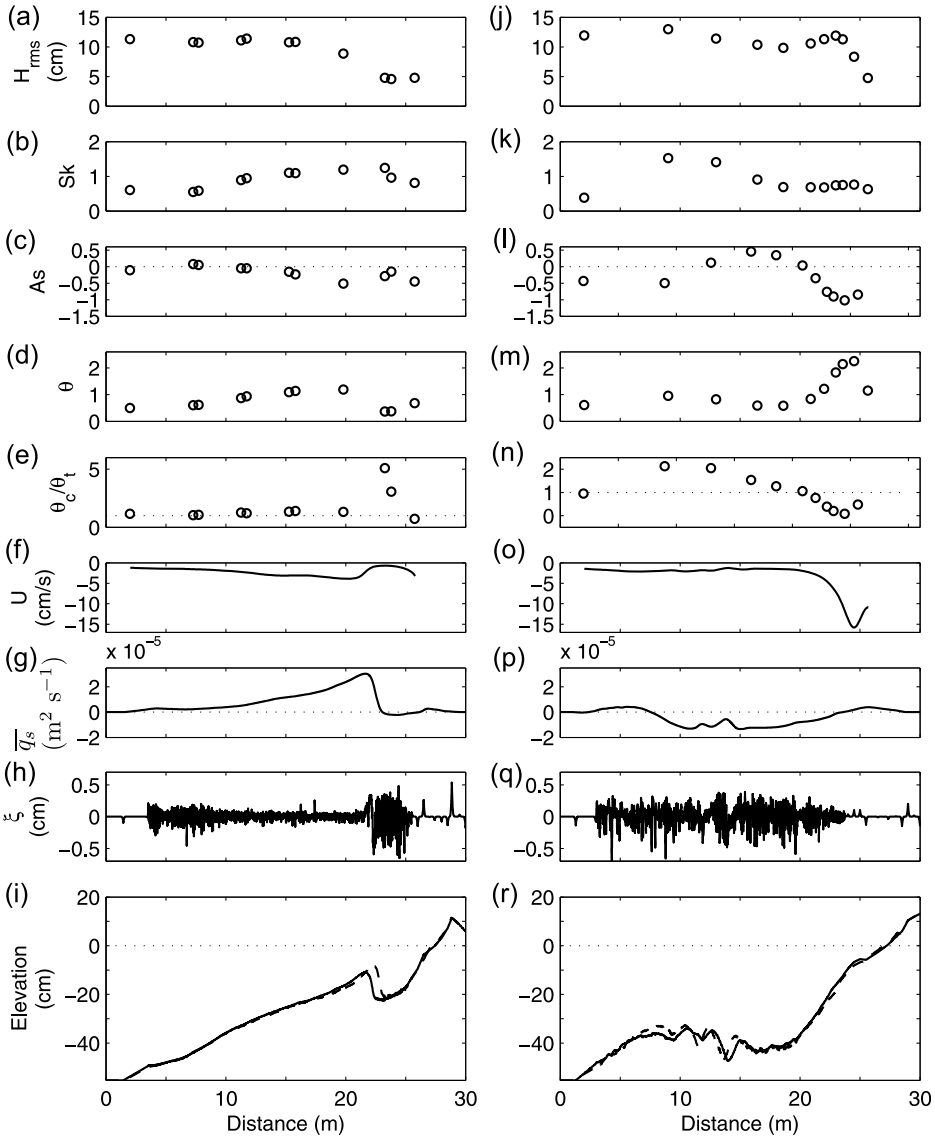

Figure 6. (a and j) Root mean square wave height H_{rms}, (b and k) wave skewness *Sk*, (c and l) wave asymmetry *As*, (d and m) Shields number θ, (e and n) ratio of crest to trough Shields numbers θ_c/θ_t, (f and o) undertow *U*, (g and p) net sediment transport rate $\overline{q_s}$, (h and q) bed level fluctuations ξ, and (i and r) initial (solid) and final (dashed) beach profiles. Figures 6a–6i show onshore bar migration (H_s = 16 cm, T_p = 2 s, experiment 1); Figures 6j–6r show offshore bar formation (H_s = 16 cm, T_p = 3 s, experiment 2).

the top of the beach profile. As shown in Figure 6d, θ is large for both large *Sk* and *As*. The ratio θ_c/θ_t peaks on the lee of the bar in Figure 6e and becomes smaller than 1 for a large undertow in Figure 6n. Most importantly, it is large (along with large *Sk*) as the sediment transport is directed offshore for $9 \leq x \leq 15$ m in Figures 6j–6r.

3.2. Wave Period Influence on Sediment Transport

[29] Using a constant sediment settling velocity w_s, the Dean number $\Omega = H_s/(T_p\, w_s)$ can be seen as the ratio H_s/T_p. Analyzing the influence of Ω on wave climates with the same H_s comes down to analyzing the influence of T_p. For a moderate significant wave height (H_s = 10.7 cm), two climates with T_p = 1.4 s (Ω = 3.6) and T_p = 2 s (Ω = 2.5) are compared (experiments 15 and 16, Figures 7a–7i). Initial beach profiles are similar. Observations of the trends reveal that the sediment transport is mainly onshore (offshore) directed for the wave climate with a shorter (longer) peak period. The incoming wave height is the same in both cases. During their propagation, long period waves become higher and then lead to a more intense breaking. As opposed to *As*, *U*, and θ which present similar signatures in both cases, *Sk* is clearly larger for longer waves (T_p = 2 s). In line with (6), for a given water depth and a constant H_{rms} in the shoaling zone, an increase in T_p increases the wave skewness.

[30] The opposite sediment flux directions observed for $15 \leq x \leq 20$ m for the two cases is mainly the result of differences in *Sk* and bed level fluctuations ξ. When *Sk* is weak and the bed is almost flat, the sediment flux is onshore directed, according to the classical concept of sediment

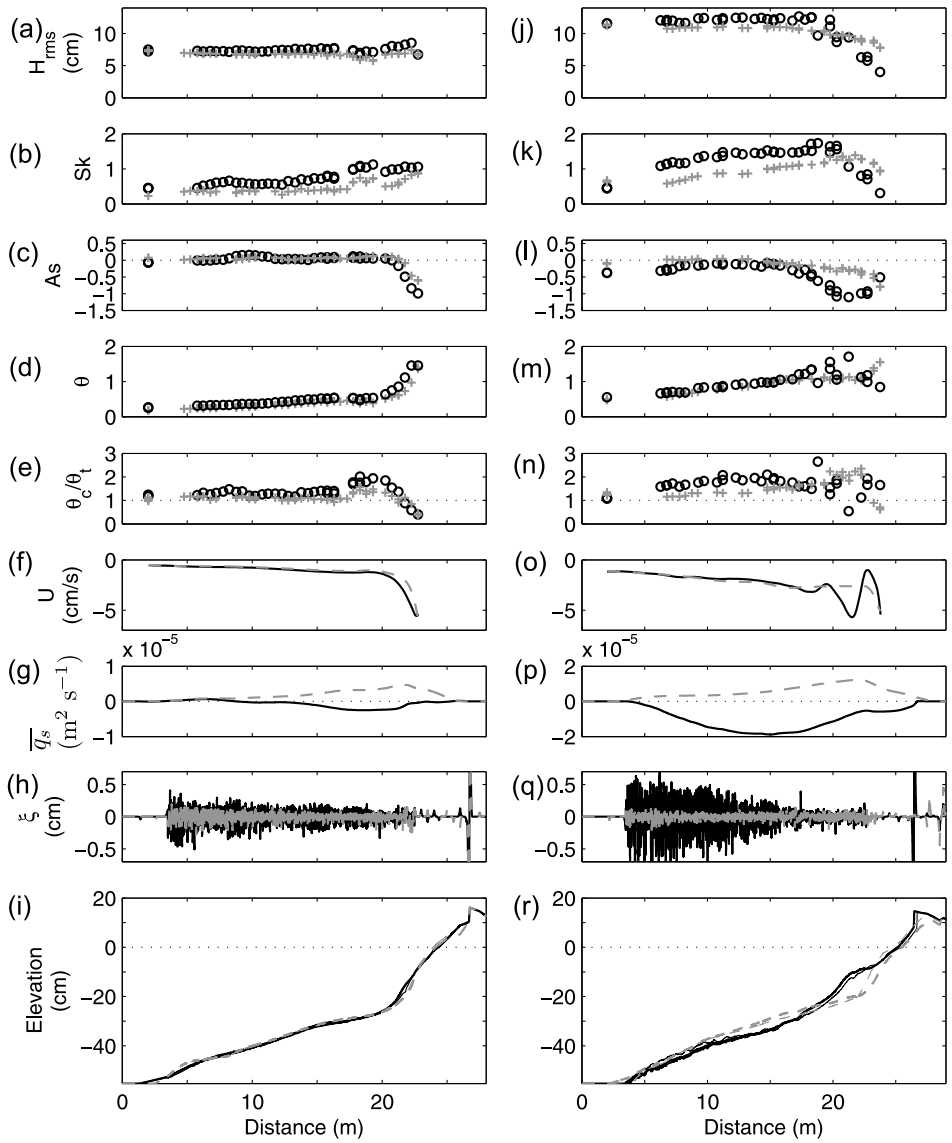

Figure 7. (a and j) Root mean square wave height H_{rms}, (b and k) wave skewness *Sk*, (c and l) wave asymmetry *As*, (d and m) Shields number θ, (e and n) ratio of crest to trough Shields numbers θ_c/θ_t, (f and o) undertow *U*, (g and p) net sediment transport rate $\overline{q_s}$, (h and q) bed level fluctuations ξ, and (i and r) initial (bold) and final (thin) beach profiles. Wave period influence on sediment transport. Figures 7a–7i show H_s = 10.7 cm, T_p = 1.4 s (gray dashed lines and pluses, experiment 15) and T_p = 2 s (black solid lines and circles, experiment 16); Figures 7a–7i show H_s = 16 cm, T_p = 2 s (dashed lines and pluses, experiment 17) and T_p = 3 s (solid lines and circles, experiment 18).

transport induced by "cnoidal" skewed waves (or second-order Stokes waves). In first approximation, the sediment transport is proportional to the orbital wave velocity [*Ribberink et al.*, 2000]. However, when *Sk* is large and the bed is more rippled, the sediment flux is offshore directed. This net offshore sediment transport cannot be the result of the undertow alone because the ratio $\theta_c/\theta_t > 1$ (Figure 7e) indicates a stronger sediment stirring under the wave crests. Besides, effects of turbulent stirring induced by the breaking waves can also be discarded here because the surf zone is limited on the top of the beach profiles ($x \geq 22$ m). The observed net offshore sediment transport can only be explained by phase-lag effects. Indeed, the sediment mobilized during the wave crest is transported by the following wave trough. Such a behavior is also observed close to x = 20 m where ripples are hardly detected and the net sediment transport is clearly offshore directed. This is in line with many authors who observed, for fine sands, a decrease in onshore sediment transport and subsequently offshore-directed fluxes as the wave skewness increases [e.g., *Ribberink et al.*, 2008; *Ruessink et al.*, 2009].

[31] A similar comparison is done for energetic wave conditions (H_s = 16 cm) in Figures 7j–7r (experiments 17 and 18). Using T_p = 2 and 3 s allows to obtain almost the same Dean numbers (3.7 and 2.5) as for the moderate wave conditions described above. Beach profiles are less similar, but the sediment transport tendencies are very close to those in Figures 7a–7i. Thus, the wave climate with a shorter

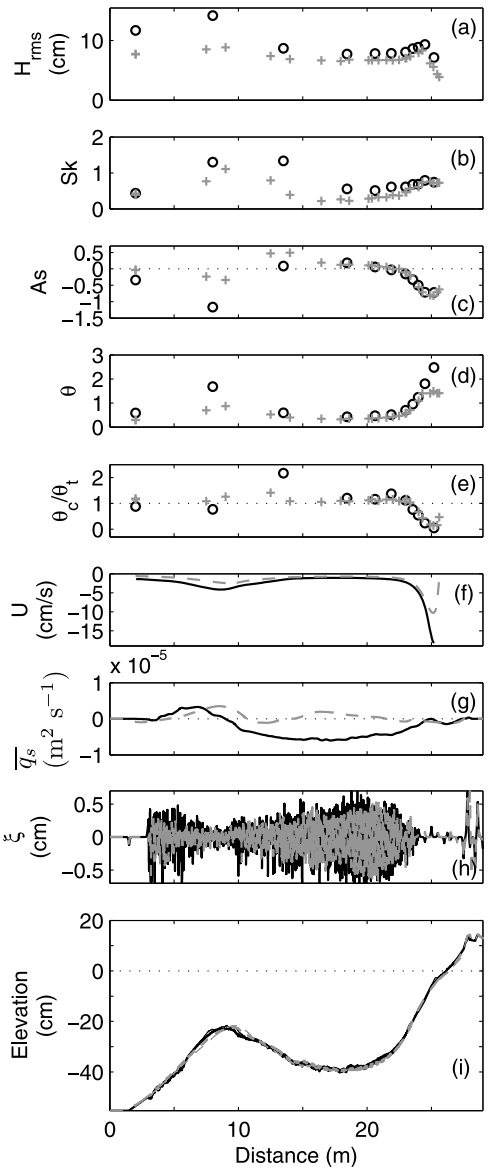

Figure 8. (a) Root mean square wave height H_{rms}, (b) wave skewness *Sk*, (c) wave asymmetry *As*, (d) Shields number θ, (e) ratio of crest to trough Shields numbers θ_c/θ_t, (f) undertow *U*, (g) net sediment transport rate $\overline{q_s}$, (h) bed level fluctuations ξ, and (i) initial (bold) and final (thin) beach profiles. Wave height influence on sediment transport: H_s = 10.7 cm, T_p = 2 s (gray dashed lines and pluses, experiment 5) and H_s = 16 cm, T_p = 3 s (black solid lines and circles, experiment 10).

(longer) peak period presents an onshore (offshore) sediment flux. Readily noticeable for $8 \le x \le 16$ m, the only significant changes which could explain the oppositing sediment flux directions observed between T_p = 2 s and T_p = 3 s, concern the wave skewness and the bed level fluctuations. As observed above, large values of wave skewness above a rippled bed, coinciding with weak wave asymmetry and undertow values here also appear to drive an offshore sediment transport. Once again, the undertow cannot be responsible of such offshore sediment transport ($\theta_c/\theta_t > 1$), but it can be explained by phase-lag effects. Conversely, the effects of a strong undertow are observed on the top of the beach.

[32] Comparing the results of experiments 16 (left, circles) and 17 (right, pluses) for $2 \le x \le 18$ m, although with similar variations of most parameters, the sediment transport is weakly offshore directed in experiment 16 (order of magnitude 2×10^{-6} m^2 s^{-1}) and onshore directed in experiment 17. This can be explained by a slightly more developed rippled bed in experiment 16 which points at the fact that ripple vortices enhance sediment mobilization and favor offshore-directed sediment transport by phase-lag effects.

3.3. Wave Height Influence on Sediment Transport

[33] The wave energy flux is defined as

$$F_w = \frac{1}{8}\,\rho\, g\, c\, H_{rms}^2 \tag{19}$$

The wave climate energy, linked to the root mean square wave height, is often applied to explain the sediment transport. To get a better understanding of its influence, in Figure 8 we compare two wave climates having the same Dean number $\Omega = 2.5$: a moderate one (B, experiment 5) and an energetic one characterized by higher and longer waves (C, experiment 10). Initial profiles are very similar barred beaches. The sediment transport associated to the energetic conditions is essentially offshore directed, except on the seaward side of the bar. This confirms the bar formation mechanism as being the result of sediment convergence, observed in Figures 6j–6r. In contrast, the sediment flux is mainly onshore directed for the moderate conditions. The same sediment onshore flux intensities are observed at x = 6.5 and 8.5 m for energetic and moderate conditions despite clear differences in wave characteristics. This indicates a competition between *Sk*, *As*, and *U* sediment transport related processes. Concerning case C, this behavior can be explained by the large wave asymmetry which promotes the sediment mobilization during the rising part of the crest velocity, whereas during the waning part the sediment settles while being transported onshore. In such asymmetric wave conditions, plug flow can also favor onshore sediment transport, especially for the energetic case with a high Shields number ($\theta \approx 2$).

[34] Incoming wave heights are clearly different for the two cases. However, they tend to have the same value in the surf zone where the waves height saturate. In case C the bar acts as a filter dissipating high wave energy. It results in larger values of *Sk*, *As*, *U*, and θ on the bar for the energetic case. Onshore of the bar, the values are close to those of the moderate case, except for *Sk*, which remains larger. For the energetic conditions, we observe offshore sediment transport in the bar trough ($15 \le x \le 20$ m), whereas the effect of the undertow is negligible ($\theta_c/\theta_t > 1$). In this zone of relatively low agitation, the bed present fully developed ripples ($0.45 \le \theta \le 0.65$). As for experiments 16 and 18 in Figure 7, the phase-lag effects induced by the large wave skewness provide plausible processes for explaining the net offshore sediment transport. The ripples contribute to this behavior, in particular at $x \approx 20$ m where *Sk* decreases significantly. For the moderate wave conditions, ripples are also observed in the bar trough but the net sediment transport is onshore directed. It means that rippled beds are not always associ-

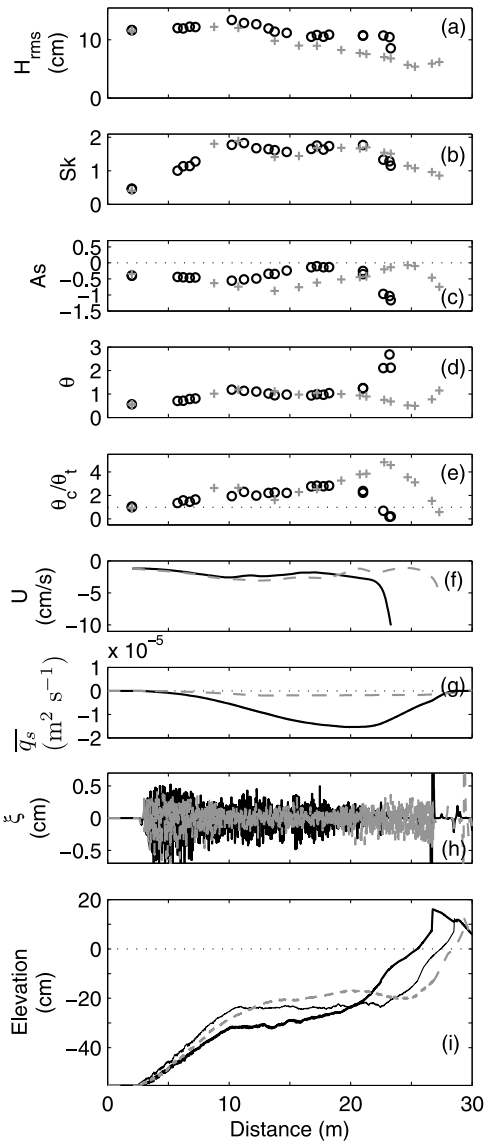

Figure 9. (a) Root mean square wave height H_{rms}, (b) wave skewness *Sk*, (c) wave asymmetry *As*, (d) Shields number θ, (e) ratio of crest to trough Shields numbers θ_c/θ_t, (f) undertow *U*, (g) net sediment transport rate $\overline{q_s}$, (h) bed level fluctuations ξ, and (i) initial (bold) and final (thin) beach profiles. For wave climate C (H_s = 16 cm, T_p = 3 s): transient (black solid lines and circles, experiment 3); and equilibrium (gray dashed lines and pluses, experiment 4) states.

ated with offshore sediment transport, in particular when the wave skewness is small.

[35] The bar formation mechanism is often described as the convergence of sediment, resulting from the onshore-directed flux due to the wave nonlinearities, and the offshore-directed flux due to the undertow [e.g., *Masselink and Hughes*, 2003]. From the above results (and those presented in Figure 6), the onshore sediment transport on the seaward side of the bar is indeed induced by the wave asymmetry, however, the offshore sediment transport that feeds the bar on its shoreward side likely results from the large wave skewness rather than from the weak undertow.

3.4. Transient and Equilibrium States

[36] The cross-shore sediment transport variations associated with transient and equilibrium states are compared in Figure 9. They are related to the wave climate C (experiments 3 and 4). The transient beach profile morphodynamics is characterized by a rapid beach face erosion, leading to the formation of a terrace ("step-like") profile. The equilibrium profile does not change substantially during 11.5 h of wave forcing. The sediment transport is clearly offshore directed for the transient state, with a maximum at $x \approx 20$ m, whereas it is almost zero for the equilibrium state. A first breaking zone starts on the step around $x \approx 10$ m, associated with similar increases in *Sk*, *As*, *U*, and θ for both states. For the transient state, the waves break again close to $x \approx 23$ m, inducing a strong undertow. The wider breaker zone for the equilibrium state induces large values of *As* for a longer distance over the terrace. However, in contrast to the bar trough in Figures 6j–6r, *Sk* remains large all across the terrace due to the relatively shallow water depth in both cases. Moreover, these experiments readily demonstrates that breaking zones are characterized by large values of both *Sk* and *As*.

[37] Although the offshore sediment transport in the transient state for $22 \le x \le 25$ m certainly results from the strong undertow, where θ_c/θ_t is smaller than 1, this is not the case for $10 \le x \le 20$ m where θ_c/θ_t is clearly larger than 1. *U*, θ, and *Sk* are almost the same as in the equilibrium case. The only noticeable difference is observed in *As*, which is clearly weaker in the transient state. As observed in Figures 7 and 8, large values of *Sk* associated with weak *As* values drive the sediment transport in offshore direction. In the equilibrium case, the high *Sk* values for $10 \le x \le 20$ m are compensated by large *As* values.

4. Discussion and Conclusions

[38] The energetic wave conditions simulated in our experiments lead mainly to offshore sediment transport, as it had been described in nature during storm events by many authors [e.g., *Ostrowski et al.*, 1990]. Experiments with lower wave conditions correspond essentially to onshore sediment fluxes, also in agreement with field observations for moderate wave climates [*King*, 1972; *Sonu and James*, 1973]. Onshore bar migration is mainly associated with onshore-directed sediment transport, whereas terrace profile and offshore bar formation correspond to offshore sediment transport. For a given significant wave height, an increase (decrease) in the wave climate peak period is associated with an increase (decrease) in wave skewness, and leads mostly to offshore (onshore) sediment fluxes.

[39] It has been hypothesized in the past that sandbar generation could be the result of sediment convergence at the nodes or antinodes of infragravity standing waves [*Carter et al.*, 1973; *Holman and Bowen*, 1982]. Despite recent attempts to evaluate the influence of long waves on sediment transport in the surf and swash zones [e.g., *Baldock et al.*, 2010], it is difficult to isolate their role from other effects such as induced breaking point and wave height variations or short wave nonlinearities modifications. In our experiments, effects of infragravity waves on sediment transport in the shoaling and surf zones were not detected. According to several authors [e.g., *Baldock et al.*, 2004;

Michallet et al., 2007; *Grasso et al.*, 2007], the infragravity waves generated by irregular wave breaking present a modal structure that depends on the beach morphology and their energy depends on the incoming significant wave height. In the cases presented in Figures 7a–7i for instance, the beach profiles and the incoming wave height are very similar that lead to very similar infragravity wave patterns. Clearly, the observed differences in sediment transport cannot be due to long waves in this case. Out of the swash zone where they probably play an important role, the infragravity waves seem to have a weak impact on sediment transport in our experiments.

[40] The wave asymmetry signatures observed in our experiments are very similar to those observed in natural beaches. *Elgar et al.* [2001] observed peaks in wave asymmetry on the bar, where waves break, and *Hoefel and Elgar* [2003] noticed secondary peaks on the beach face. Field measurements presenting large wave skewness should be further analyzed in the light of the present findings. To our knowledge, offshore sediment transport associated to a large velocity skewness and a weak undertow has not been identified yet in natural sites.

[41] Sediment transport beneath skewed asymmetric oscillatory flows above a plane bed was simulated by *Ruessink et al.* [2009] using a 1DV-RANS "advection/diffusion" model. This study shows that, for fine sands ($d_{50} = 0.12$ mm), the sediment transport can reverse from the offshore direction, due to the wave skewness, to the onshore direction by an increase in wave asymmetry.

[42] In the present experiments sediment transport mechanisms cover bed load, ripple, and sheet flow regimes. While not described in details, processes such as turbulent stirring and plug flow occurrence are implicitly accounted for in this study. Turbulent stirring is associated to large wave asymmetries and undertow in the breaking zone, as well as plug flow that likely occurs for high values of the Shields number. The experiments are fully characterized by an unsteady behavior, implying important phase-lag effects. The sediment transport associated with beach changes is greatly affected by the interaction between wave skewness and asymmetry. An original concept, by its application to skewed asymmetric irregular waves, is summed up in the following. For small skewness values, the sediment flux is onshore directed. In this situation the sediment is weakly mobilized and the crest velocities which exceed the trough velocities produce an onshore flux. The wave asymmetry additionally contributes to the transport in the same direction. For larger wave skewness, either the wave asymmetry is weak and the sediment is transported offshore (crest-to-trough phase-lag effects), or the wave asymmetry is large enough (trough-to-crest phase-lag effects) to reverse the trend and transports the sediment onshore. It is clearly observed that, for given wave characteristics, the presence of ripples increases the net sediment transport in the offshore direction. This concept fits relatively well to the experiments. Except at the top of the beach, the sediment transport direction in our experiments seems to be more influenced by the wave nonlinearities rather than the undertow. This suggests that wave skewness plays an important role in bar formation and offshore migration. The vertical structure of the velocity skewness close to the bed should also be further investigated to better assess the sediment transport forcing [*Henderson et al.*, 2004]. As a prospect, numerical modeling of sediment transport forced by irregular waves should provide interesting quantitative results to confront with the present experimental ones.

[43] **Acknowledgments.** This study was funded by the SHOM/INSU-RELIEFS MODLIT project, the ECOS-Sud program with CONYCIT, and the French Ministry of Defense (DGA/DS 2009.60.077). The technical assistance of J.-M. Barnoud is gratefully acknowledged. We particularly acknowledge the reviewers for their constructive comments and Timothy Price for his valuable corrections.

References

Aagaard, T., K. P. Black, and B. Greenwood (2002), Cross-shore suspended transport in the surf zone: A field-based parametrization, *Mar. Geol.*, *185*, 283–302.

Bagnold, R. A. (1963), Mechanics of marine sedimentation, in *The Earth Beneath the Sea, The Sea*, vol. 3, edited by M. N. Hill, pp. 507–528, Wiley-Intersci., New York.

Bagnold, R. A. (1966), An approach to the sediment transport problem from general physics, *U.S. Geol. Surv. Prof. Pap.*, *442-I*, 37 pp.

Bailard, J. A. (1981), An energetics total load sediment transport model for a plane sloping beach, *J. Geophys. Res.*, *86*, 10,938–10,954.

Baldock, T. E., T. J. O'Hare, and D. A. Huntley (2004), Long wave forcing on a barred beach, *J. Fluid Mech.*, *503*, 321–343.

Baldock, T. E., P. Manoonvoravong, and K. S. Pham (2010), Sediment transport and beach morphodynamics induced by free long waves, bound long waves and wave groups, *Coastal Eng.*, *57*, 898–916.

Bowen, A. J., D. L. Inman, and V. P. Simmons (1980), Simple models of nearshore sedimentation: Beach profiles and longshore bars, in *The Coastline of Canada*, edited by S. B. McCann, *Geol. Surv. Can. Pap.*, 80–10, 1–11.

Camenen, B. (2009), Estimation of the wave-related ripple characteristics and induced bed shear stress, *Estuarine Coastal Shelf Sci.*, *84*, 553–564.

Carter, T. G., P. L. F. Liu, and C. C. Mei (1973), Mass transport by waves and offshore sand bedforms, *J. Waterw. Harbors Coastal Eng. Div. Am. Soc. Civ. Eng.*, *99*, 165–184.

Castelle, B., V. Marieu, P. Bonneton, N. Bruneau, and F. Grasso (2010), Modélisation des évolutions de profil de plage, *La Houille Blanche Rev. Int. de L'eau*, *1*(13), 104–110.

Cienfuegos, R., E. Barthélemy, and P. Bonneton (2010), A wave-breaking model for Boussinesq-type equations including roller effects in the mass conservation equation, *J. Waterw. Port Coastal Ocean Eng.*, *136*(1), 10–26.

Dally, W. R., and C. A. Brown (1995), A modelling investigation of the breaking wave roller with application to cross-shore currents, *J. Geophys. Res.*, *100*, 24,873–24,883.

Davies, A. G., L. C. van Rijn, J. S. Damgaard, J. van de Graaff, and J. S. Ribberink (2002), Intercomparison of research and practical sand transport models, *Coastal Eng.*, *46*, 1–23.

Dibajnia, M., and A. Watanabe (1992), Sheet flow under nonlinear waves and currents, in *Coastal Engineering 1992: Proceedings of the Twenty-Third International Conference, October 4–9, 1992 in Venice, Italy*, pp. 2015–2028, Am. Soc. of Civ. Eng., New York.

Doering, J. C., and A. J. Bowen (1995), Parametrization of orbital velocity asymmetries of shoaling and breaking waves using bispectral analysis, *Coastal Eng.*, *26*, 15–33.

Dohmen-Janssen, C. M., D. F. Kroekenstoel, W. N. Hassan, and J. S. Ribberink (2002), Phase lags in oscillatory sheet flow: Experiments and bed load modelling, *Coastal Eng.*, *46*, 61–87.

Drake, T. G., and J. Calantoni (2001), Discrete particle model for sheet flow sediment transport in the nearshore, *J. Geophys. Res.*, *106*, 19,859–19,868.

Elgar, S., E. L. Gallagher, and R. T. Guza (2001), Nearshore sandbar migration, *J. Geophys. Res.*, *106*, 11,623–11,628.

Foster, D. L., A. J. Bowen, R. A. Holman, and P. Natoo (2006), Field evidence of pressure gradient induced incipient motion, *J. Geophys. Res.*, *111*, C05004, doi:10.1029/2004JC002863.

Gallagher, E. L., S. Elgar, and R. T. Guza (1998), Observation of sand bar evolution on a natural beach, *J. Geophys. Res.*, *103*, 3203–3215.

Grasso, F. (2009), Modélisation physique de la dynamique hydro-sédimentaire des plages, Ph.D. thesis, 170 pp., Univ. Joseph Fourier, Grenoble, France.

Grasso, F., H. Michallet, and E. Barthélemy (2007), Infragravity waves in modile-bed laboratory experiments, in *Coastal Sediment 07: Proceedings of the Sixth International Symposium on Coastal Engineering and Science of Coastal Sediment Process, May 13–17, 2007, New Orleans, Louisiana*, pp. 235–247, Am. Soc. of Civ. Eng., Reston, Va.

Grasso, F., H. Michallet, E. Barthélemy, and R. Certain (2009a), Physical modeling of intermediate cross-shore beach morphology: Transients and equilibrium states, *J. Geophys. Res.*, *114*, C09001, doi:10.1029/2009JC005308.

Grasso, F., H. Michallet, R. Certain, and E. Barthélemy (2009b), Experimental flume simulation of sandbar dynamics, *J. Coastal Res.*, *SI56*, 54–58.

Grasso, F., H. Michallet, and E. Barthélemy (2011), Experimental simulation of shoreface nourishments under storm events: A morphological, hydrodynamic, and sediment grain size analysis, *Coastal Eng.*, *58*, 184–193.

Hanes, D., V. Alymov, Y. Chang, and C. Jette (2001), Wave-formed ripples at Duck, North Carolina, *J. Geophys. Res.*, *106*, 22,575–22,592.

Henderson, S. M., J. S. Allen, and P. A. Newberger (2004), Nearshore sandbar migration predicted by an eddy-diffusive boundary layer model, *J. Geophys. Res.*, *109*, C06024, doi:10.1029/2003JC002137.

Hoefel, F., and S. Elgar (2003), Wave-induced sediment transport and sandbar migration, *Science*, *299*(5614), 1885–1887.

Holman, R. A., and A. J. Bowen (1982), Bars, bumps, and holes: Models for the generation of complex beach topography, *J. Geophys. Res.*, *87*, 457–468.

Hsu, T. J., and D. M. Hanes (2004), Effects of wave shape on sheet flow sediment transport, *J. Geophys. Res.*, *109*, C05025, doi:10.1029/2003JC002075.

Hsu, T. J., S. Elgar, and R. T. Guza (2006), Wave-induced sediment transport and onshore sandbar migration, *Coastal Eng.*, *53*, 817–824.

Kennedy, A. B., Q. Chen, J. T. Kirby, and R. A. Dalrymple (2000), Boussinesq modelling of wave transformation, breaking and runup. I: 1D, *J. Waterw. Port Coastal Ocean Eng.*, *126*(1), 39–48.

King, C. A. M. (1972), *Beaches and Coasts*, Edward Arnold, London.

Madsen, O. S. (1974), Stability of a sand bed under breaking waves, in *Coastal Engineering 1974: Proceedings of the Fourteenth Coastal Engineering Conference, June 24–28, Copenhagen, Denmark*, pp. 776–794, Am. Soc. of Civ. Eng., New York.

Marino-Tapia, I. J., P. E. Russell, T. J. O'Hare, M. A. Davidson, and D. A. Huntley (2007), Cross-shore sediment transport on natural beaches and its relation to sandbar migration patterns: 1. Field observations and derivation of a transport parameterization, *J. Geophys. Res.*, *112*, C03001, doi:10.1029/2005JC002893.

Masselink, G., and M. G. Hughes (2003), *An Introduction of Coastal Processes and Geomorphology*, Oxford Univ. Press, Oxford, U. K.

Masselink, G., M. J. Austin, T. J. O'Hare, and P. E. Russell (2007), Geometry and dynamics of wave ripples in the nearshore zone of a coarse sandy beach, *J. Geophys. Res.*, *112*, C10022, doi:10.1029/2006JC003839.

Michallet, H., F. Grasso, and E. Barthélemy (2007), Long waves and beach evolution profiles, *J. Coastal Res.*, *SI50*, 221–225.

Michallet, H., R. Cienfuegos, E. Barthélemy, and F. Grasso (2011), Kinematics of waves propagating and breaking on a barred beach, *Eur. J. Mech. B*, doi:10.1016/j.euromechflu.2010.12.004, in press.

Nielsen, P. (1992), *Coastal Bottom Boundary Layers and Sediment Transport*, *Adv. Ser. Ocean Eng.*, vol. 4, World Sci., Singapore.

O'Donoghue, T., J. S. Doucette, J. J. van der Werf, and J. S. Ribberink (2006), The dimensions of sand ripples in full-scale oscillatory flows, *Coastal Eng.*, *53*, 997–1012.

Ostrowski, R., Z. Pruszak, and R. B. Zeidler (1990), Multi-scale nearshore and beach changes, in *Coastal Engineering 1990: Proceedings of the Twenty-Second Coastal Engineering International Conference, July 2–6, 1990 in Delft, The Netherlands*, pp. 2101–2116, Am. Soc. of Civ. Eng., New York.

Pape, L., Y. Kuriyama, and B. G. Ruessink (2010a), Models and scales for cross-shore sandbar migration, *J. Geophys. Res.*, *115*, F03043, doi:10.1029/2009JF001644.

Pape, L., N. G. Plant, and B. G. Ruessink (2010b), On cross-shore migration and equilibrium states of nearshore sandbars, *J. Geophys. Res.*, *115*, F03008, doi:10.1029/2009JF001501.

Ribberink, J. S., and A. A. Al-Salem (1994), Sediment transport in oscillatory boundary layers in cases of rippled beds and sheet flow, *J. Geophys. Res.*, *99*, 707–727.

Ribberink, J. S., C. M. Dohmen-Janssen, D. M. Hanes, S. R. McLean, and C. Vincent (2000), Near-bed sand transport mechanisms under waves, a large-scale flume experiment (Sistex99), in *Coastal Engineering 2000: Proceedings of the Twenty-First Coastal Engineering International Conference, July 16–21, 2000 in Sydney, Australia*, pp. 3263–3276, Am. Soc. of Civ. Eng., Reston, Va.

Ribberink, J. S., J. J. van der Werf, T. O'Donoghue, and W. N. M. Hassan (2008), Sand motion induced by oscillatory flows: Sheet flow and vortex ripples, *J. Turbulence*, *9*(20), 1–32.

Roelvink, J. A., and M. J. F. Stive (1989), Bar-generating cross-shore flow mechanisms on a beach, *J. Geophys. Res.*, *94*, 4785–4800.

Ruessink, B. G., Y. Kuriyama, A. J. H. M. Reniers, J. A. Roelvink, and D. J. R. Walstra (2007), Modeling cross-shore sandbar behavior on the timescale of weeks, *J. Geophys. Res.*, *112*, F03010, doi:10.1029/2006JF000730.

Ruessink, B. G., T. J. J. van den Berg, and L. C. van Rijn (2009), Modeling sediment transport beneath skewed asymmetric waves above a plane bed, *J. Geophys. Res.*, *114*, C11021, doi:10.1029/2009JC005416.

Ruessink, B. G., H. Michallet, T. Abreu, F. Sancho, D. A. van der A, J. van der werf, and P. A. Silva (2011), Observations of velocities, sand concentrations, and fluxes under velocity-asymmetric oscillatory flows, *J. Geophys. Res.*, doi:10.1029/2010JC006443, in press.

Scott, N. V., T. J. Hsu, and D. Cox (2009), Steep wave, turbulence, and sediment concentration statistics beneath a breaking wave field and their implications for sediment transport, *Cont. Shelf Res.*, *29*, 2303–2317.

Silva, P. A., T. Abreu, D. A. van der A, F. Sancho, B. G. Ruessink, J. J. van der Werf, and J. S. Ribberink (2011), Sediment transport in nonlinear skewed oscillatory flows: the transkew experiments, *J. Hydraul. Res.*, in press.

Sleath, J. F. A. (1999), Conditions for plug formation in oscillatory flow, *Cont. Shelf Res.*, *19*, 1643–1664.

Sonu, C. J., and W. R. James (1973), A Markov model for beach profile changes, *J. Geophys. Res.*, *78*, 1462–1471.

Swart, D. H. (1974), A schematization of onshore-offshore transport, in *Coastal Engineering 1974: Proceedings of the Fourteenth Coastal Engineering Conference, June 24–28, Copenhagen, Denmark*, pp. 884–900, Am. Soc. of Civ. Eng., New York.

Terrile, E., A. J. H. M. Reniers, M. J. F. Stive, M. Tromp, and H. J. Verhagen (2006), Incipient motion of coarse particles under regular shoaling waves, *Coastal Eng.*, *53*, 81–92.

van der A, D. A., T. O'Donoghue, and J. S. Ribberink (2010), Measurements of sheet flow transport in acceleration-skewed oscillatory flow and comparison with practical formulations, *Coastal Eng.*, *57*, 331–342.

van der Werf, J. J., J. S. Doucette, T. O'Donoghue, and J. S. Ribberink (2007), Detailed measurements of velocities and suspended sand concentrations over full-scale ripples in regular oscillatory flow, *J. Geophys. Res.*, *112*, F02012, doi:10.1029/2006JF000614.

van Thiel de Vries, J. S. M., M. R. A. van Gent, D. J. R. Walstraa, and A. J. H. M. Reniers (2008), Analysis of dune erosion processes in large-scale flume experiments, *Coastal Eng.*, *55*, 1028–1040.

Yu, X., T. J. Hsu, and D. M. Hanes (2010), Sediment transport under wave groups: Relative importance between nonlinear waveshape and nonlinear boundary layer streaming, *J. Geophys. Res.*, *115*, C02013, doi:10.1029/2009JC005348.

E. Barthélemy and H. Michallet, Laboratoire des Ecoulements Géophysiques et Industriels, UJF/G-INP/CNRS, BP 53, F-38041 Grenoble CEDEX, France. (eric.barthelemy@hmg.inpg.fr; herve.michallet@hmg.inpg.fr)

F. Grasso, Institute for Marine and Atmospheric Research, Department of Physical Geography, Faculty of Geosciences, Utrecht University, PO Box 80115, 3508 TC Utrecht, Netherlands. (f.grasso@geo.uu.nl)